Transitions to valence-bond solid order in a honeycomb lattice antiferromagnet

Sumiran Pujari,[1,2] Fabien Alet,[1] and Kedar Damle[3]
[1]*Laboratoire de Physique Théorique, IRSAMC, Université de Toulouse, CNRS, 31062 Toulouse, France*
[2]*Department of Physics, University of Kentucky, Lexington, Kentucky 50406, USA*
[3]*Department of Theoretical Physics, Tata Institute of Fundamental Research, Mumbai 400 005, India*
(Received 5 February 2015; revised manuscript received 5 March 2015; published 16 March 2015)

We use quantum Monte Carlo methods to study the ground-state phase diagram of a $S = 1/2$ honeycomb lattice magnet in which a nearest-neighbor antiferromagnetic exchange J (favoring Néel order) competes with two different multispin interaction terms: a six-spin interaction Q_3 that favors columnar valence-bond solid (VBS) order, and a four-spin interaction Q_2 that favors staggered VBS order. For $Q_3 \sim Q_2 \gg J$, we establish that the competition between the two different VBS orders stabilizes Néel order in a large swath of the phase diagram even when J is the smallest energy scale in the Hamiltonian. When $Q_3 \gg (Q_2, J)$ $[Q_2 \gg (Q_3, J)]$, this model exhibits at zero temperature phase transition from the Néel state to a columnar (staggered) VBS state. We establish that the Néel-columnar VBS transition is continuous for all values of Q_2, and that critical properties along the entire phase boundary are well characterized by critical exponents and amplitudes of the noncompact CP^1 ($NCCP^1$) theory of deconfined criticality, similar to what is observed on a square lattice. However, a surprising threefold anisotropy of the phase of the VBS order parameter at criticality, whose presence was recently noted at the $Q_2 = 0$ deconfined critical point, is seen to persist all along this phase boundary. We use a classical analogy to explore this by studying the critical point of a three-dimensional XY model with a fourfold anisotropy field which is known to be weakly irrelevant at the three-dimensional XY critical point. In this case, we again find that the critical anisotropy appears to saturate to a nonzero value over the range of sizes accessible to our simulations.

DOI: 10.1103/PhysRevB.91.104411 PACS number(s): 75.10.Jm, 05.30.Rt, 75.10.Kt

I. INTRODUCTION

Ground states of quantum antiferromagnets with $S = 1/2$ moments on a two-dimensional (2d) bipartite lattice (such as square or honeycomb lattices) generally exhibit long-range spin correlations at the Néel wave vector $\mathbf{Q}$ [1]. This $T = 0$ antiferromagnetic order, encoded in a nonzero value of the Néel order parameter vector $\vec{n}$, can be destroyed by frustrating further-neighbor [2–8] or ring-exchange interactions, as well as by certain more tractable multispin couplings designed [9] to partially mimic the effect of such frustrating interactions. In many examples, the resulting phase has no magnetic order and instead exhibits spatial ordering of the bond energy. In such a bond-ordered valence-bond solid (VBS) state [10], the singlet projector $P_{\langle ij\rangle} = -\vec{S}_i \cdot \vec{S}_j + 1/4$ of two nearest-neighbor spins $\langle ij\rangle$ has an expectation value that exhibits spatial structure at the VBS ordering wave-vector(s) $\mathbf{K}$, resulting in a nonzero value for the complex VBS order parameter ψ.

A standard Landau approach (based on a coarse-grained free-energy density [11] expressed in terms of powers of $\vec{n}$ and ψ and their space-time gradients) would predict that this phase transformation generically proceeds either via a direct first-order transition, or via two continuous transitions separated by an intermediate phase which has both orders or no order. Since the latter possibilities are more exotic, the simplest generic possibility within Landau theory is thus a direct first-order transition. Such first-order behavior is indeed observed in square [12] and honeycomb lattice [13] spin models where a multispin interaction drives the system to a staggered VBS state [Fig. 1(b)].

The theory of deconfined quantum critical points [14–16] proposed by Senthil *et al.* argues that such Landau-theory considerations are misleading when the transition is towards a state with columnar VBS order [Fig. 1(a)] on the square or honeycomb lattice. Indeed, their arguments [14–16] strongly suggest that such transitions can be generically (without fine-tuning any parameter) second-order in nature. In this alternate approach, one writes the partition function as an imaginary-time (τ) path integral over space-time configurations $\vec{n}(\vec{r},\tau)$, and notes that the spatial configuration $\vec{n}(\vec{r})$ on a given time slice admits topological skyrmion textures in spatial dimension $d = 2$. The corresponding total skyrmion number is conserved during the imaginary-time evolution as long as the space-time configuration of $\vec{n}$ remains nonsingular. Conversely, when the skyrmion number-changing operator $\Psi_{\vec{R}}$ acts at imaginary time τ on plaquette $\vec{R}$, it creates a hedgehog defect centered at $\vec{R},\tau$. In this path-integral representation, this hedgehog defect carries a Berry phase $2\pi p(\vec{R})/q$ where $p(\vec{R}) = 0,1,\ldots,q-1$ depends on the sublattice to which $\vec{R}$ belongs and $q = 3$ ($q = 4$) for the honeycomb (square) lattice case [17–20].

Remarkably, this phase factor ensures that the transformation properties of Ψ under lattice symmetries are identical to those of the complex VBS order parameter ψ for columnar order on both honeycomb and square lattices [14,15,18,19]. The two operators can thus be identified with each other insofar as their long-distance correlations are concerned [here and henceforth, we refer to ψ as the "columnar" order parameter, although ψ is also nonzero if the system has plaquette VBS order as shown in Fig. 1(a) for the honeycomb lattice case]. The destruction of Néel order in the ground state can be described as a proliferation of such hedgehog defects, providing a natural mechanism for a direct transition between Néel and columnar VBS orders [14–16]. This theoretical description only involves q-fold ($q = 3$ on the honeycomb lattice and $q = 4$ on the square lattice) hedgehogs (corresponding to Ψ^q and its Hermitian conjugate), as defects with smaller hedgehog

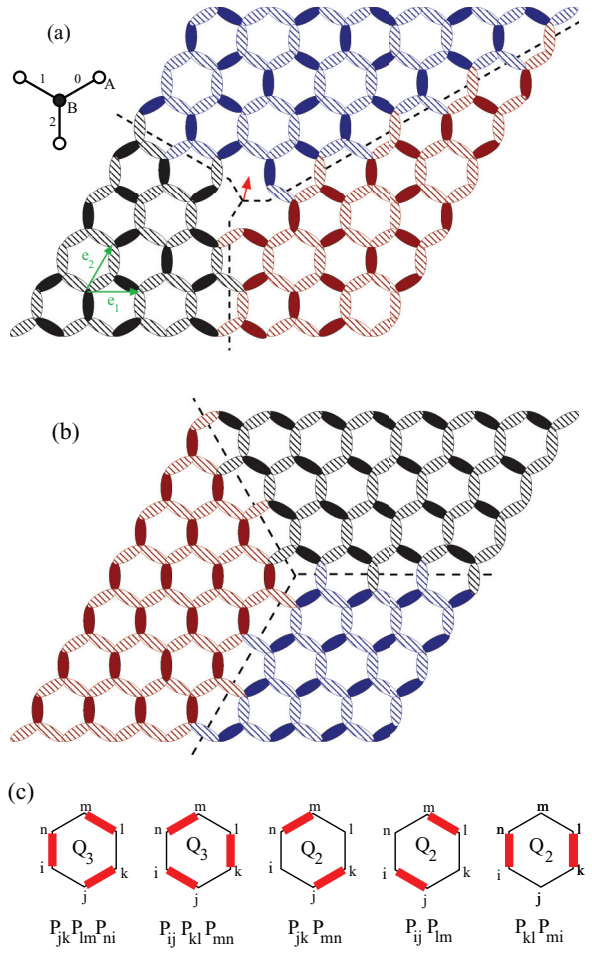

FIG. 1. (Color online) (a) Columnar VBS order on the honeycomb lattice: dark links represent higher values of $\langle P_l \rangle$ (the singlet projection operator on this link) than light links. If dark links are instead reinterpreted as representing lower values of P_l, one obtains a representation of plaquette VBS order at the same wave vector. (b) Staggered VBS order on the honeycomb lattice, where again dark links represent higher values of $\langle P_l \rangle$. In both panels, we have created different ordered domains (represented by different colors and separated by dashed lines) by introducing a defect. As already discussed [13], the defect has a spinful core (a free spin $1/2$ sits at the domain wall intersection) for columnar/plaquette VBS whereas the core is spinless for the staggered VBS. Also shown are our conventions for labeling unit cells $\vec{r}$, bonds μ belonging to unit cells $\vec{r}$, and A and B sublattice sites in unit cell $\vec{r}$. (c) Schematic representations of the four- and six-spin interaction terms Q_2 and Q_3.

number carry rapidly oscillating Berry phases, causing the corresponding terms in the action to scale to zero upon coarse-graining. Such restrictions on hedgehog charges in space-time configurations of $\vec{n}$ are best analyzed [21] in the CP^1 representation $\vec{n} = z_\alpha^* \vec{\sigma}_{\alpha\beta} z_\beta$, where z_α is a two-component complex field and $\vec{\sigma}$ the vector of Pauli matrices. In the CP^1 representation, hedgehogs correspond to monopoles in the compact $U(1)$ gauge field to which the z_α are minimally coupled [21–23]. Thus, if the corresponding *noncompact* CP^1 theory ($NCCP^1$) has a second-order transition, and if threefold (fourfold) monopoles are irrelevant perturbations at the corresponding monopole-free fixed point, one expects the Néel-columnar VBS transition on the honeycomb (square) lattice to be generically continuous, with critical properties in the $NCCP^1$ universality class [14–16]. Conversely, if threefold (fourfold) monopoles are relevant at the putative $NCCP^1$ critical point, the simplest scenario is that this leads to runaway flows which signal weakly first-order behavior for the Néel-columnar VBS transition on the honeycomb (square) lattice [14–16].

To understand the scaling behavior of q-fold monopole creation operators in the vicinity of the noncompact CP^1 critical point, it is instructive to consider a more general $NCCP^{N-1}$ theory which has N-component fields z_α and study the limiting behavior of q-fold monopole perturbations in the $N = 1$ and $N = \infty$ limits. For instance, fourfold monopoles are known to be irrelevant both at $N = 1$ [14,19,24–26] and $N = \infty$ [14,19,24], making it very likely that they are also irrelevant in the physical $N = 2$ case [14–16]. Thus, the Néel-columnar VBS transition on the square lattice is expected to be generically second order, with critical properties described by the $NCCP^1$ theory [14–16].

The behavior of threefold monopoles at the noncompact CP^1 critical point is harder to understand from such a study of limiting cases. This is because the physical $N = 2$ case lies between the $N = 1$ case where threefold monopoles are *relevant* [14,19,24,25] and lead to a weakly first-order transition [27], and the $N = \infty$ [14,19,24] limit where they are irrelevant. These contrasting behaviors in the two limits makes it difficult to argue one way or the other concerning the behavior of threefold monopole perturbations at the $N = 2$ critical point [14–16]. A nice summary of the expected behavior of the $NCCP^{N-1}$ theory with q-fold monopoles (including results of numerical simulations) can be found in Ref. [28].

This theory of deconfined criticality has motivated several numerical studies [28–45] of model quantum Hamiltonians designed [9] to host a Néel-VBS columnar transition. In parallel work, other studies have tried to access the physics of deconfined criticality in three-dimensional classical models [45–55]. On the square lattice (with $q = 4$), QMC simulations [28–31,33–37,39,40,42,44,45] find no direct signature of first-order behavior even at the largest sizes studied. This is true both for SU(2) symmetric models, as well as spin models with enhanced SU(N) symmetry, which are expected to exhibit a transition in the $NCCP^{N-1}$ universality class. Further, critical properties fit reasonably well to standard scaling predictions for second-order transitions [28–30,33–37,39,44]. The corresponding values of η_N and η_D, the anomalous exponents governing power-law decays of the Néel order parameter $\vec{n}$ and the VBS order parameter ψ, are relatively large [28,40,44], as expected from the theory of deconfined criticality. Additionally, the numerically estimated critical exponents for large values of N [using lattice spin models with SU(N) symmetry] approach the limiting values obtained in a large-N expansion of the $NCCP^{N-1}$ theory [28,39,56]. Further, different "designer Hamiltonians" with different multispin couplings [29,34,39] yield the same estimates for exponents and critical amplitudes. At or close to this critical point, histograms of the phase of ψ exhibit near-perfect $U(1)$ symmetry [29,33,40], consistent with the idea that the

irrelevance of the fourfold monopole insertion operator Ψ^4 implies, via the identification $\Psi \sim \psi$, the irrelevance of the fourfold anisotropy in the phase of the VBS order parameter ψ. However, in the SU(2) case, slow (perhaps logarithmic) drifts with increasing linear size L are clearly visible [31,34–37,45] in certain dimensionless quantities which are expected to be scale invariant at a conventional second-order critical point in three space-time dimensions; examples include the spin stiffness and vacancy-induced spin textures. Since histograms of phase of ψ exhibit $U(1)$ symmetry characteristic of the noncompact theory, it seems plausible that these drifts are intrinsic properties of the noncompact critical point. This interpretation is supported by the fact that Monte Carlo simulations of a lattice-regularized NCCP^1 theory [45–47] also see some drifts that mar otherwise convincing scaling behavior (it is also possible to find different lattice-regularizations that lead to a first-order behavior [45–47]). However, at the present juncture, there is no detailed understanding of these drifts that goes beyond this reasonable guess (see however the recent analytical arguments of Refs. [57,58]). Finally, we caution that some authors [31,45] have also interpreted these drifts as either hints of a very weak first-order transition, or as the signature of a flow towards a new universality class different from NCCP^1.

What about the honeycomb lattice case ($q = 3$)? Recent numerical studies of tractable model Hamiltonians provide a fairly consistent picture of a direct second-order transition between the Néel and the columnar VBS states [28,43,44], with numerical estimates of the anomalous exponents η_N and η_D, correlation length exponent ν, and universal scaling functions [44] all consistent, within errors, with the best estimates for the square-lattice transition. Further, slow drifts in spin stiffness analogous to the square lattice case have also been observed at the putative critical point [43]. All this strongly suggests that the honeycomb lattice transition is also described by the NCCP^1 theory of deconfined criticality.

However, our recent work has also identified an important new feature of the honeycomb lattice transition [43]: if the honeycomb lattice transition is indeed described by the NCCP^1 theory, threefold monopoles must be irrelevant at the NCCP^1 critical point. Since $\Psi \sim \psi$, this would imply that threefold anisotropy in the phase of the VBS order parameter ψ is irrelevant at criticality. However, it was found [43] that dimensionless measures of this threefold anisotropy at criticality appear to saturate to a nonzero value as a function of increasing size (at least for the sizes at which numerical calculations were feasible, which are comparable with those used in square lattice studies). The simplest explanation is that tripled monopoles are irrelevant with a very small scaling dimension, meaning that the dimensionless critical threefold anisotropy should flow to zero very slowly. If one only has access to data over a limited range of sizes, it can appear to saturate at a nonzero value.

The present study aims at clarifying this issue of anisotropy, as well as adding some further numerical evidence for the less documented case of deconfined criticality on the honeycomb lattice, relevant for frustrated honeycomb lattice spin models [4–7]. In this context, we note that a recent study [59] suggests an interesting experimental realization of deconfined criticality in bilayer graphene in magnetic and electric fields, further adding to our motivation for studying the Néel-columnar VBS transition on the honeycomb lattice.

We focus here on a numerically tractable model in which the nearest-neighbor antiferromagnetic exchange J competes with two different multispin interaction terms, a six-spin interaction Q_3 that favors a columnar VBS state (when $Q_3 \gg Q_2, J$), and a four-spin interaction Q_2 that favors a staggered VBS (when $Q_2 \gg Q_3, J$). The deconfined quantum critical point for the model at $Q_2 = 0$ has been studied in our previous work [43], as well as in Ref. [44]. The motivation for perturbing this model with the Q_2 term was threefold: (i) This new energy scale (when not too large) will introduce a critical line of $Q_{3c}(Q_2)$ for the Néel-columnar VBS phase boundary. Universality of critical exponents and amplitudes can be tested along this critical line [66]. (ii) If Q_2 tunes the "bare" value of the threefold anisotropy of the columnar VBS order parameter ψ, one could test the behavior of the critical threefold anisotropy along the phase boundary line $Q_{3c}(Q_2)$. (iii) The competition between the staggered and columnar VBS orders in the regime $Q_2 \sim Q_3 \gg J$ may reveal exotic physics: the transition from staggered VBS order (with maximal winding in the valence-bond pattern) to columnar VBS order (with zero winding) may proceed through an intervening quantum spin liquid (where no winding sector is favored).

Before proceeding further, it is useful to summarize the key findings of the present work: (i) We establish that the transition from Néel to columnar VBS order is continuous for all values of Q_2, and that critical properties along the entire Néel-columnar VBS phase boundary $Q_{3c}(Q_2)$ are well characterized by critical exponents and amplitudes of the NCCP^1 theory of deconfined criticality. (ii) The threefold anisotropy of the phase of the VBS order parameter persists all along this phase boundary, with slight but perceptible *upward drift* in its value as Q_2 is increased. To explore the possibility that this may reflect the fact that tripled monopoles are irrelevant with a very small scaling dimension, we use a classical analogy and study the critical point of the 3d XY model with a fourfold anisotropy field which is known to be irrelevant with a small scaling dimension [25,60]. Our results for the dimensionless anisotropy on this classical model are qualitatively similar to our results for the threefold anisotropy at the Néel-columnar VBS transition: in both cases, the anisotropy appears to saturate to a nonzero value over the available range of sizes, although, in the classical case, one expects it to be irrelevant at the transition. (iii) For $Q_3 \sim Q_2 \gg J$, the competition between these two different VBS orders does not lead to an intervening spin-liquid phase. Rather, it stabilizes Néel order in a large swath of the phase diagram even when J is the smallest energy scale in the problem.

The article is organized as follows: In Sec. II, we introduce the J-Q_3-Q_2 models that we will study and provide some computational details. In Sec. III, we show our estimates for the phase boundaries in the (Q_2, Q_3) plane. In Sec. IV, we study in greater detail the nature of phase boundary $Q_{3c}(Q_2)$ separating the Néel phase and the columnar VBS phase, including the behavior of the threefold anisotropy in the phase of the columnar VBS order parameter. In Sec. V, we study the classical three-dimensional XY model with fourfold

anisotropy. Finally, we conclude in Sec. VI with a brief discussion about possible directions for future work. Some additional numerical results (on the finite-size scaling analysis of critical anisotropy, as well as the 3d XY model with $q = 3$-, 5-fold anisotropic fields) are relegated to Appendices A and B.

II. MODEL AND METHODS

The main focus of our work is the numerical study of a model of spin-1/2 moments on sites of the honeycomb lattice, coupled by a nearest-neighbor exchange J that competes with a four-spin interaction Q_2 and a six-spin interaction Q_3:

$$\begin{aligned} H &= H_J + H_{Q_3} + H_{Q_2}, \\ H_J &= -J \sum_{\langle ij \rangle} P_{\langle ij \rangle}, \\ H_{Q_3} &= -Q_3 \sum_{\langle ijklmn \rangle} P_{\langle ij \rangle} P_{\langle kl \rangle} P_{\langle mn \rangle} + P_{\langle jk \rangle} P_{\langle lm \rangle} P_{\langle ni \rangle}, \\ H_{Q_2} &= -Q_2 \sum_{\langle ijklmn \rangle} P_{\langle ij \rangle} P_{\langle lm \rangle} + P_{\langle jk \rangle} P_{\langle mn \rangle} + P_{\langle kl \rangle} P_{\langle ni \rangle}, \end{aligned} \tag{1}$$

where $P_{\langle ij \rangle} = 1/4 - \mathbf{S}_i \cdot \mathbf{S}_j$ is the singlet projector on the bond $\langle i, j \rangle$ and $\langle ijklmn \rangle$ denotes an elementary hexagon with vertices labeled cyclically [Fig. 1(c)]. We set $J = 1$ so that all energies are measured in units of J. This model is studied using the same techniques as in Ref. [43], for both obtaining the ground state and characterizing its physical properties. We summarize them here for completeness, using the same notations: we use a QMC projector algorithm [61] on honeycomb lattices of linear size up to $L = 60$, consisting of L^2 unit cells with two spins corresponding to the two-sublattice structure of the honeycomb lattice. Periodic boundary conditions are imposed.

Néel order is characterized using the vector order parameter $\vec{M} = \frac{1}{2L^2} \sum_{\vec{r}} \vec{n}(\vec{r})$, with $\vec{n}$ the local Néel field $\vec{n}(\vec{r}) = \vec{S}_{\vec{r}A} - \vec{S}_{\vec{r}B}$. The unit cell is labeled by $\vec{r}$ and subscripts A and B refer to the two sites in this unit cell located on the different sublattices. The VBS order at the columnar wave vector $\mathbf{K} \equiv (2\pi/3, -2\pi/3)$ is characterized by the order parameter $\psi = \frac{1}{2L^2} \sum_{\vec{r}} V_{\vec{r}}$, where $V_{\vec{r}}$ is the local field:

$$V_{\vec{r}} = (P_{\vec{r}0} + e^{2\pi i/3} P_{\vec{r}1} + e^{4\pi i/3} P_{\vec{r}2}) e^{i\mathbf{K}\cdot\vec{r}},$$

with $P_{\vec{r}\mu}$ ($\mu = 0,1,2$) the singlet projector on one of the three bonds μ corresponding to the unit cell labeled by $\vec{r}$ (see Fig. 1). This definition implies a phase of 0, $2\pi/3$, and $4\pi/3$ for ψ for the three symmetry-related pure columnar ordered VBS (Fig. 1), and $\pi/3$, π, and $5\pi/3$ for ψ for the three symmetry-related pure plaquette ordered VBS (Fig. 1). Finally, to quantify the staggered VBS order, we follow Ref. [13] and use the nematic order parameter $\phi = \frac{1}{2L^2} \sum_{\vec{r}} W_{\vec{r}}$, where $W_{\vec{r}}$ is the local staggered VBS order parameter field, written as

$$W_{\vec{r}} = (P_{\vec{r}0} + e^{2\pi i/3} P_{\vec{r}1} + e^{4\pi i/3} P_{\vec{r}2}).$$

Note the absence of any $\vec{r}$-dependent phase factor in this definition. This is consistent with the fact that staggered VBS order only breaks the symmetry of threefold rotations, while preserving translational symmetry.

To detect quantum phase transitions, we consider the square of the modulus of the three order parameters of interest: $\langle \vec{M}^2 \rangle$, $\langle |\psi|^2 \rangle = \langle \psi^\dagger \psi \rangle$, and $\langle |\phi|^2 \rangle = \langle \phi^\dagger \phi \rangle$. For a continuous Néel-columnar VBS transition, we expect the scaling forms $\langle \vec{M}^2 \rangle = L^{-(1+\eta_N)} f_{\vec{M}}((Q_3 - Q_{3c}^N) L^{1/\nu_N})$ and $\langle |\psi|^2 \rangle = L^{-(1+\eta_{\rm VBS})} f_\psi((Q_3 - Q_{3c}^D) L^{1/\nu_D})$. In writing these scaling forms, we assume that the phase boundary is crossed by varying Q_3 at fixed Q_2 and allow for two different correlation length exponents $\nu_{N/D}$ associated with Néel/columnar VBS correlations at different critical values $Q_{3c}^{N/D}$. We do not quote the scaling form for the staggered VBS order as this transition is strongly first order.

We also use the Binder ratios $g_M = \langle (\vec{M}^2)^2 \rangle / \langle \vec{M}^2 \rangle^2$, $g_\psi = \overline{|E_\psi|^4} / (\overline{|E_\psi|^2})^2$, and $g_\phi = \overline{|E_\phi|^4} / (\overline{|E_\phi|^2})^2$ to locate the quantum critical points where Néel, columnar, and staggered VBS orders respectively disappear. The two first Binder ratios are expected to scale close to a continuous quantum phase transition as $g_M = g_M((Q_3 - Q_{3c}^N) L^{1/\nu_N})$ and $g_\psi = g_\psi((Q_3 - Q_{3c}^D) L^{1/\nu_D})$, respectively. Note that both VBS Binder ratios are not written in terms of the powers of the corresponding VBS order parameter, as this would involve computations of eight-spin correlation functions, for which there is no simple expression in the valence-bond formalism used in the QMC simulations. Instead, we use moments of the Monte Carlo estimator E_ψ [29,33] (respectively E_ϕ), whose *Monte Carlo* average $\overline{E_\psi}$ (respectively $\overline{E_\phi}$) coincides with the *quantum-mechanical* expectation value $\langle \psi \rangle$ ($\langle \phi \rangle$) of the columnar (resp. staggered) VBS order parameter. Explicit description of the related Monte Carlo measurements can be found in Ref. [29]. In all our simulations, we found that this correctly reproduces the expected physical behavior for moments of ψ or ϕ.

Close to continuous quantum phase transitions, we have fitted our numerical data to the respective scaling forms, using a polynomial up to second order in most cases for the universal functions $f_{M/\psi}$ and $g_{M/\psi}$.

We now introduce the observables related to the phase of the columnar VBS order parameter ψ. The phase of ψ distinguishes a fixed columnar (Kekulé) pattern of bond-energy expectation values from one in which a sublattice of plaquettes hosts a valence-bond resonance (see Fig. 1). Both patterns correspond to a threefold symmetry breaking and lead to order at the same wavevector $\mathbf{K}$, but they differ in the phase of the complex VBS order parameter ψ. In our QMC simulations, we do not have access strictly speaking to the phase of ψ, but rather to the phase θ_{E_ψ} of the estimator $E_\psi \equiv |E_\psi| \exp(i\theta_{E_\psi})$. We nevertheless expect that it reflects the behavior of the true phase of ψ. We recall that our definition of ψ leads θ_{E_ψ} to take 0, 2π,3, and $4\pi/3$ for the three symmetry-related columnar VBS, while θ_{E_ψ} takes $\pi/3$, π, and $5\pi/3$ for the three symmetry-related plaquette VBS. To address the relevance of threefold monopole events, we consider the following dimensionless measure of the anisotropy in the distribution of this phase:

$$W_3 = \int dE_\psi \, P(E_\psi) \cos(3\theta_{E_\psi}), \tag{2}$$

where $P(E_\psi)$ is the normalized probability distribution for this quantity as sampled by the Monte Carlo run. W_3 thus takes a value of 1 for a pure columnar VBS when θ_{E_ψ} is 0, $2\pi/3$, or

$4\pi/3$ in any superposition, while it takes a value of -1 for a pure plaquette VBS when θ_{E_ψ} is $\pi/3$, π, or $5\pi/3$ in any superposition. In the total absence of phase anisotropy, W_3 takes a value of 0.

It is also possible to analyze our data using scaling theories [25,26,64] to capture the finite-size behavior of W_3 near criticality. We have used such a scaling analysis to fit our numerical data as detailed in Appendix A, but we prefer to display the bare numerical data for the anisotropy measure W_3 in Sec. IV B in order to avoid any assumption regarding the scaling form obeyed by W_3.

III. PHASE DIAGRAM

We first present our results on the phase diagram of the ground state of H in the (Q_2, Q_3) plane. As noted earlier, H_J favors Néel ordering, while H_{Q_2} (H_{Q_3}) favors staggered (columnar) VBS order. We can locate two limiting points using results from previous works. The model $H_J + H_{Q_3}$ has been shown [43] to host a continuous phase transition from the Néel to a columnar VBS state at $Q_{3c}(Q_2 = 0) \simeq 1.19$. Since Q_2 disfavors columnar VBS order, we expect the phase boundary $Q_{3c}(Q_2)$ between the Néel state and the columnar VBS state to define an increasing function of Q_2, at least for small Q_2. On the other hand, Ref. [13] showed that the model $H_J + H_{Q_2}$ exhibits a strongly first-order transition from the Néel to the staggered VBS state at $Q_{2c}(Q_3 = 0) \simeq 6.4$. We expect the first-order transition to staggered VBS order to shift to increasing values of Q_2 when Q_3 is turned on.

A first estimate on the location of these phase boundaries is given by the magnitude of the Néel Binder cumulant g_M. In our definition of g_M, and for a large enough system size, a value close to 1 corresponds to a phase with antiferromagnetic order, while a value $5/3$ corresponds to Gaussian fluctuations centered at zero, signaling no magnetic order. At the quantum Néel-columnar VBS critical point at $Q_2 = 0$, the Néel Binder cumulant takes [43] a value $\simeq$1.42 (which should be universal), lying between these two limiting values. In contrast, close to a first-order transition [62], this Binder cumulant can take values larger than $5/3$ on finite systems. We display the magnitude of g_M for a system of moderate size $L = 24$ in the top panel of Fig. 2. This allows a first estimate of the phase boundaries: we clearly observe two transition lines emerging from the limiting points at $Q_3 = 0$ and $Q_2 = 0$. The nature of the transitions does not appear to change, since we observe very high values for g_M (signaling a first-order transition) for the line emerging from $Q_2^c(Q_3 = 0)$, and intermediate values (between 1 and $5/3$) for the line emerging from $Q_3^c(Q_2 = 0)$, signaling a continuous transition. This is confirmed by a finite-size scaling analysis in the next section. From this study of g_M, we also see that antiferromagnetism survives in the region $Q_2, Q_3 \gg J$. Thus, the competition between the two VBS orders does not lead to spin-liquid behavior. Rather, it allows antiferromagnetism to set in although J is the smallest energy scale in the Hamiltonian. The phases where no antiferromagnetism is present are naturally expected to host columnar (at low Q_2) and staggered (low Q_3) VBS orders. This is well confirmed by the low values (close to 1) taken by the columnar and staggered VBS Binder cumulants displayed in the middle and bottom panels of Fig. 2.

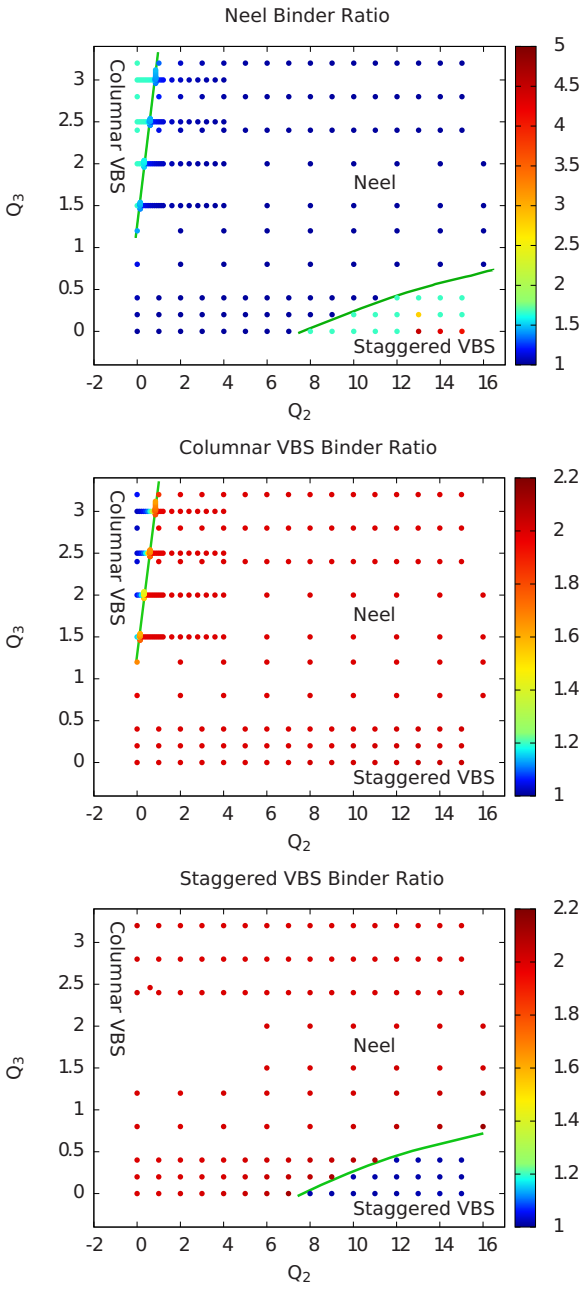

FIG. 2. (Color online) Color maps of Binder cumulants (top: Néel Binder cumulant g_M, middle: VBS columnar Binder cumulant g_ψ, bottom: staggered Binder cumulant g_ϕ) for different values in the (Q_2, Q_3) parameter space, for a system of linear size $L = 24$. Low values indicate long-range order, while high values indicate absence of order. These results allow us to map the phase diagram where Néel, columnar, and staggered VBS phases can be identified (green lines are indications of approximate phase boundaries).

We now consider more carefully the transition line $Q_{2c}(Q_3)$ between the Néel and staggered VBS order, by locating the abrupt first-order jumps in the two order parameters. An example of these jumps is shown in Fig. 3 and the resulting phase boundary is represented as a line in Fig. 2. The transition between the Néel and columnar VBS transitions deserves a more careful finite-size scaling analysis, which is presented

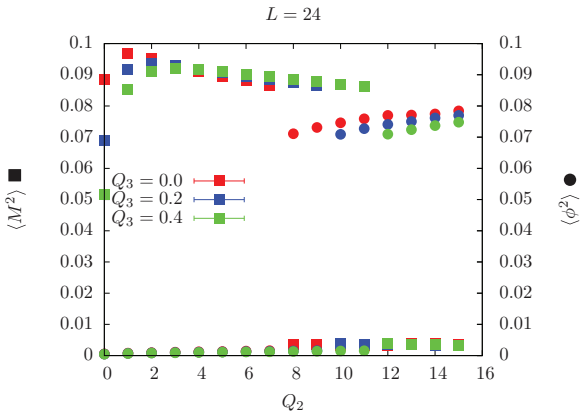

FIG. 3. (Color online) The first-order transition from Néel to staggered VBS order is readily identified by the sharp jumps in the corresponding order parameters (filled squares for $\langle M^2 \rangle$ shown on left y axis, filled circles for $\langle \phi^2 \rangle$ shown on right y axis), for three values of Q_3 (system size $L = 24$).

in Sec. IV: the resulting transition line $Q_{3c}(Q_2)$ is also represented in Fig. 2.

IV. NÉEL-COLUMNAR VBS TRANSITION LINE

A. Exponents and scaling forms

We focus here on the nature of the phase boundary between the Néel and the columnar VBS states. Following our earlier work [43] at $Q_2 = 0$, we locate the point at which Néel order is lost using the dimensionless Binder ratio g_M, and the point at which the columnar VBS order turns on using the corresponding Binder ratio g_ψ. For four different values of Q_2, we vary Q_3 to locate the quantum phase transition and attempt to collapse the Binder ratio data onto the corresponding scaling forms (see Sec. II). In the analysis, we allow these two scaling forms to use different values of Q_{3c} as well as different correlation length exponents ν_N and ν_D. We also analyze the collapse of the modulus squares of order parameters $\langle M^2 \rangle$ and $\langle |\psi^2| \rangle$ according to the forms in Sec. II, providing estimates of Q_{3c}, ν_N, ν_D as well as η_N and η_D.

In Figs. 4 and 5, we provide representative examples of the results of such an analysis. Our data all along the Néel-columnar VBS phase boundary are well described by conventional scaling forms. For ready reference, we also tabulate estimates of the corresponding critical points, exponents, and amplitude values obtained using these different observables in Table I.

We find that these estimates of Q_{3c} at a given value of Q_2 agree approximately with each other within statistical errors. More precisely, the spread in the best-fit values of Q_{3c} obtained from VBS data in two different ways (from g_ψ and $\langle |\psi^2| \rangle$) is of the same order as the difference in the best-fit Q_{3c} values obtained from scaling collapses of g_ψ and g_M. The same is true for the correlation length exponents ν_N and ν_D at a given value of Q_2. Therefore, we conclude that one can consistently account for all the data at a given value of Q_2 in terms of a single critical point $Q_{3c}(Q_2)$ at which Néel order is lost and columnar VBS order turns on, with both Néel and columnar order parameters controlled by a single correlation length

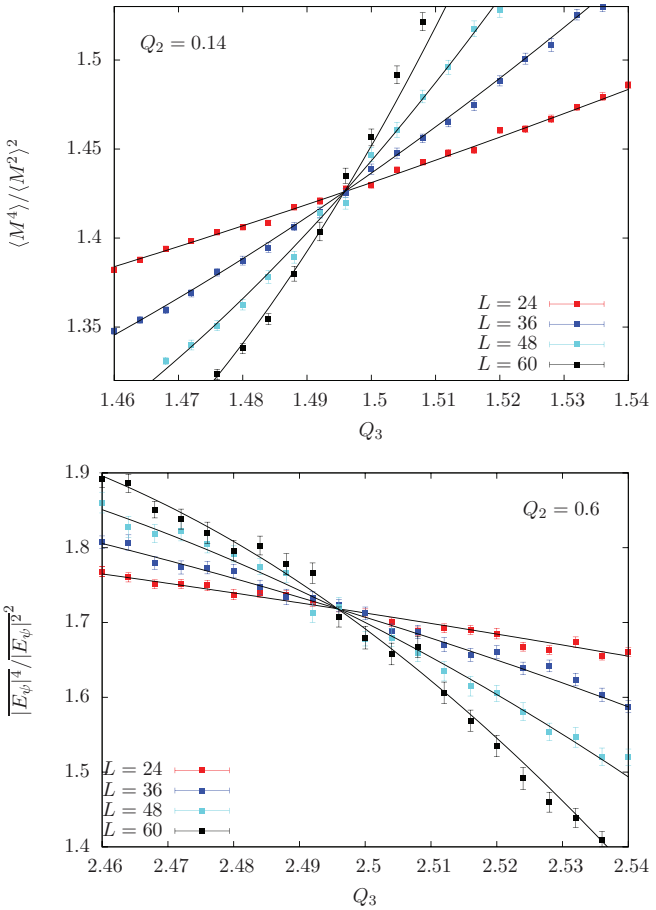

FIG. 4. (Color online) Crossing plot of Binder cumulants for different system sizes: Néel cumulant g_M (top panel, for $Q_2 = 0.14$) and columnar VBS cumulant g_ψ (bottom panel, for $Q_2 = 0.60$). Symbols are QMC data, solid lines fits to the finite-size scaling form (see text). For the fits, a particular choice of critical window, minimum system size included, and order of universal function has been shown here which gave χ^2 per degree of freedom equal to 1.53 and 0.97 for the plots respectively. For estimates on overall error bars, refer to Table I.

exponent ν. Within errors, this estimate of ν does not exhibit any Q_2 dependence. The anomalous exponents η_N and η_D are also found to be Q_2-independent within error bars (which are larger for η_D). Additionally, we note that η_N and η_D are close to each other in value (although the theory of deconfined criticality does not predict that these anomalous dimensions are equal). The amplitudes of both VBS and Binder ratios at criticality are also found to be constant within errors along the critical line. Finally, we emphasize that all estimates of the critical exponents and amplitudes for $Q_2 \neq 0$ agree with those found in the case $Q_2 = 0$ [43].

Our numerical simulations therefore indicate that the entire Néel-columnar VBS transition line belongs to a single universality class. Our estimates for the critical exponents are very close to the latest estimates for SU(2) models on the square lattice [28,40,44] suggesting that both honeycomb and square lattice transitions are in the same universality class, presumably described by the NCCP[1] critical theory. This strongly suggests that threefold monopole events are irrelevant

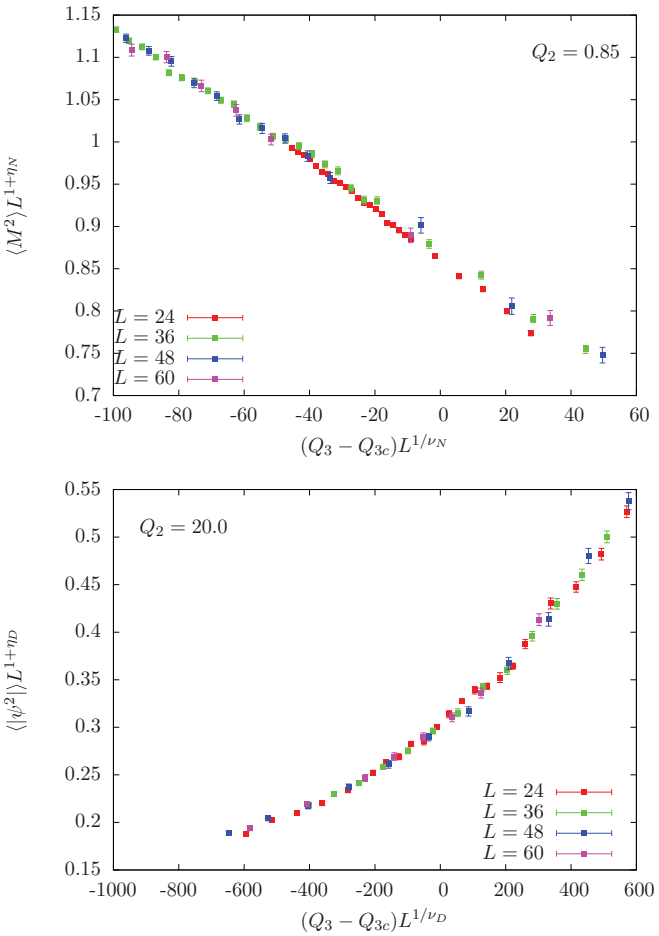

FIG. 5. (Color online) Scaling collapse for different system sizes of the Néel order parameter $\langle M^2 \rangle$ (top panel, $Q_2 = 0.85$) and columnar VBS order parameter $\langle |\psi|^2 \rangle$ (bottom panel, $Q_2 = 20.0$) in the critical region. Critical point Q_{3c} and critical exponents are obtained by fits to the standard finite-size scaling forms (see text). For the fits, again a particular choice of critical window, minimum system size included, and order of universal function has been shown here which gave χ^2 per degree of freedom equal to 1.25 and 1.15 for the plots respectively. For estimates on overall error bars, refer to Table I.

at the Néel-columnar VBS critical point for an SU(2) model on the honeycomb lattice.

B. Threefold anisotropy at criticality

Given that the entire phase boundary appears to be controlled by a single fixed point, it is of interest to investigate the Q_2 dependence of the threefold anisotropy in the phase of the columnar VBS order parameter ψ at criticality. To this end, we focus on the histogram of E_ψ measured at and in the close vicinity of our best estimate for $Q_{3c}(Q_2)$. The simplest methodology is one that requires the fewest theoretical assumptions about the scaling properties of the threefold anisotropy. In this approach, we simply monitor the large-L behavior of the dimensionless anisotropy measure W_3 (as defined in Sec. II) for a few values in the vicinity of $Q_{3c}(Q_2)$ for various values of Q_2. This L dependence is interpreted by noting that W_3 tends to zero (respectively to unity) with increasing system size deep in the Néel (resp. columnar VBS) phase. If threefold anisotropy is irrelevant at the transition, one would expect W_3 to tend to zero for large L at the critical point, but increase with increasing L when one moves into the VBS phase.

In Fig. 6, we display the L dependence of this quantity in the vicinity of $Q_{3c}(Q_2)$ for three different values of Q_2, two small and one large. From this data, it is clear that our earlier finding [43], of an apparently nonzero large-L limit for this quantity at criticality, remains valid all along the Néel-VBS phase boundary, including at the largest value of Q_2 studied. This nonzero limiting value W_{3c} appears to increase slightly with Q_2, as can already be observed in Fig. 6. A critical window around W_{3c} can be defined by considering the values taken by this dimensionless anisotropy in the critical region around Q_{3c} obtained from the analysis of the previous section. In this window, one can attempt a more sophisticated scaling analysis that uses some assumptions about the structure of the scaling theory for W_3. This is presented in Appendix A, and provides independent estimates of W_{3c} from fits to a scaling form. These estimates and the resulting conclusions are consistent with those presented above from the more direct analysis above.

We are thus led to two conclusions that appear, at first sight, to contradict each other. The first is that critical exponents and values of Binder cumulants at criticality along the entire phase boundary are compatible with the NCCP[1] universality class. The second is that this is accompanied by a nonvanishing threefold anisotropy of the phase of ψ at criticality, which furthermore appears to vary (albeit slightly) along the critical line. As we show in the next section, in the better-understood classical example of a 3d XY model with weakly irrelevant fourfold anisotropy, the dimensionless anisotropy at criticality

TABLE I. For different values of Q_2: estimates of critical point, exponent, and amplitudes resulting from the finite-size scaling analysis of order parameters $\langle M^2 \rangle$, $\langle |\psi|^2 \rangle$ and associated Binder cumulants $\langle M^4 \rangle / \langle M^2 \rangle^2$, $\langle \overline{|E_\psi|^4} \rangle / \langle \overline{|E_\psi|^2} \rangle^2$. Error bars were determined from the spread on extracted fit parameters depending on critical window size, minimum system sizes included, and degree of polynomial for the universal scaling functions, with χ^2 per degree of freedom always $\lesssim 1.5$.

	$\langle M^2 \rangle$			$g_M = \langle M^4 \rangle / \langle M^2 \rangle^2$			$\langle \|\psi\|^2 \rangle$			$g_\psi = \langle \overline{\|E_\psi\|^4} \rangle / \langle \overline{\|E_\psi\|^2} \rangle^2$		
Q_2	Q_{3c}	ν_N	η_N	Q_{3c}	ν_N	$g_M(0)$	Q_{3c}	ν_D	η_D	Q_{3c}	ν_D	$g_\psi(0)$
0.14	1.496(2)	0.58(2)	0.27(3)	1.496(1)	0.57(3)	1.425(2)	1.483(2)	0.59(2)	0.37(3)	1.491(1)	0.57(3)	1.718(5)
0.60	2.506(2)	0.56(2)	0.31(2)	2.500(1)	0.56(2)	1.427(1)	2.491(5)	0.57(3)	0.23(7)	2.495(1)	0.56(2)	1.721(3)
0.85	3.058(2)	0.55(4)	0.33(2)	3.050(2)	0.56(2)	1.428(3)	3.03(1)	0.60(3)	0.26(8)	3.044(2)	0.56(2)	1.721(5)
20.0	45.3(1)	0.57(2)	0.31(3)	45.27(2)	0.56(2)	1.430(2)	45.0(1)	0.61(3)	0.32(6)	45.18(1)	0.56(2)	1.727(1)

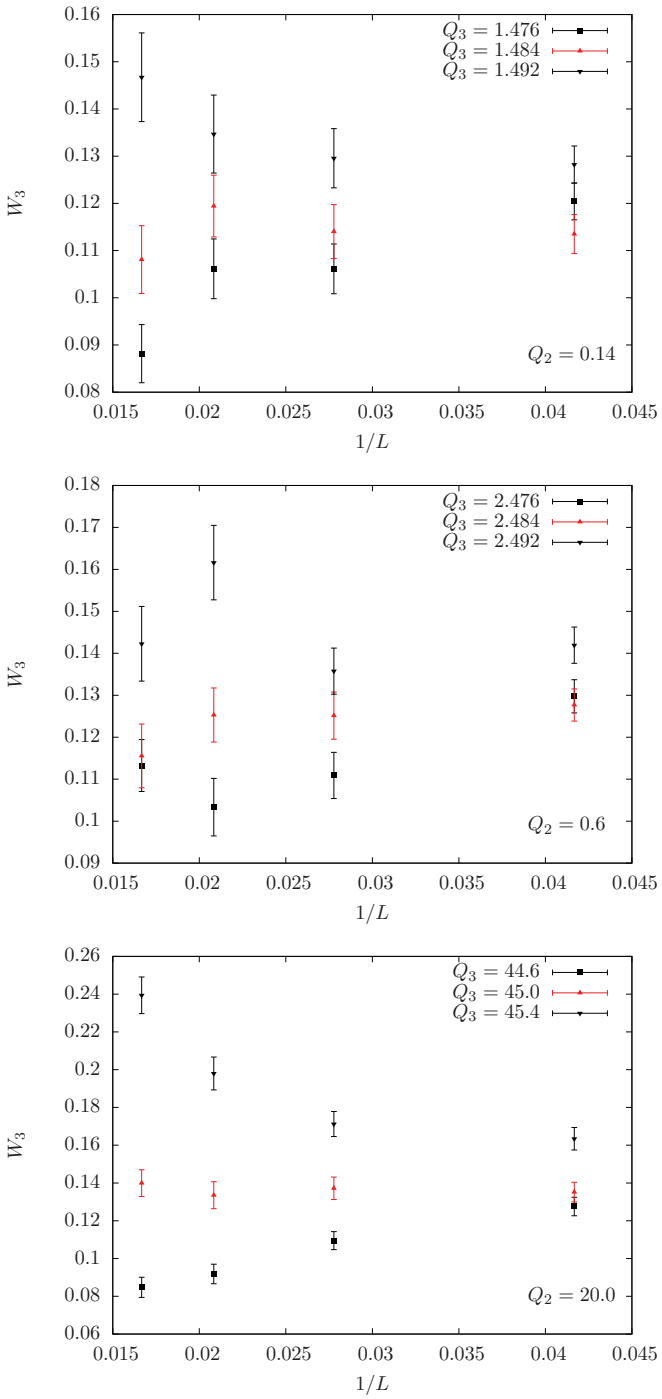

FIG. 6. (Color online) Finite-size dependence of W_3 close to the critical point for $Q_2 = 0.14$ (top panel), $Q_2 = 0.60$ (middle panel), $Q_3 = 20.0$ (bottom panel). In each case, we display data for one value of Q_3 closer to our estimate of Q_{3c}, one slightly above and one slightly below.

again appears to saturate to a nonzero large-L limit when studied over a limited range of sizes accessible to Monte Carlo simulations. As argued in the next section, this suggests a possible rationalization of our findings: threefold anisotropy is indeed irrelevant at the Néel-columnar VBS transition, but only very weakly so.

V. CLASSICAL 3d *XY* MODEL WITH Z_4 ANISOTROPY ON THE CUBIC LATTICE

We find it useful to compare this peculiar, apparently nonzero large-L limit of W_3 at criticality to the behavior of an analogous quantity in a much simpler classical setting in which one can explicitly tune the bare value of the corresponding anisotropy, namely the 3d-*XY* model with Z_4 anisotropy on the cubic lattice. This choice of analogy is dictated by the following considerations: from earlier work, we know that Z_3 anisotropy is relevant at the isotropic 3d-*XY* transition, driving the system to a weakly first-order transition, while Z_4 and higher anisotropies have all been found to be irrelevant at the isotropic *XY* transition (with Z_4 anisotropy having the smallest scaling dimension among the irrelevant terms). These conclusions are based on an ϵ expansion of the corresponding field theory [25], Monte Carlo estimates of the scaling dimensions of q-fold anisotropy terms [60], as well as direct numerical simulations of the 3d-*XY* model with $Z_{q\geqslant 4}$ anisotropies (as, e.g., in Ref. [26]) and of the $q = 3$ states Potts model [27].

Thus, by adding a Z_4 anisotropy field h_4 to the isotropic 3d-*XY* model and studying the critical point as a function of h_4, we can study an example of critical behavior in the presence of an irrelevant anisotropy which scales to zero very slowly (since it has a small scaling dimension). This provides us a setting to explore via analogy the possibility that the nonzero W_{3c} observed for all Q_2 along the Néel-columnar VBS phase boundary could reflect the fact that threefold anisotropy is irrelevant at this transition, but has small enough scaling dimension that it appears almost marginal (saturating to a nonzero value) in the range of sizes accessible to numerics.

We consider the 3d classical ferromagnetic *XY* model with a Z_4 anisotropy term, defined by the Hamiltonian

$$\mathcal{H} = -\sum_{\langle \vec{r},\vec{r}'\rangle} \cos(\theta_{\vec{r}} - \theta_{\vec{r}'}) - h_4 \sum_{\vec{r}} \cos(4\theta_{\vec{r}}), \qquad (3)$$

where $\langle \vec{r},\vec{r}'\rangle$ denotes nearest-neighbor sites on the simple cubic lattice and $\theta_{\vec{r}}$ are $U(1)$ angular variables $\in [0,2\pi)$ at site $\vec{r}$. This model has a high-temperature paramagnetic phase where the $U(1)$ symmetry is unbroken, and a low-temperature ordered phase where the spins align in one of the 4 preferred directions. At $h_4 = 0$, the model has a $U(1)$ symmetry which is spontaneously broken in the low-temperature phase. To access this physics, we perform classical Monte Carlo simulations on simple cubic lattices of linear sizes $L \in \{8,16,24,32,48,64\}$ with periodic boundary conditions using a combination of local Metropolis and Wolff cluster updates [63].

We first locate the critical points by a standard scaling analysis for four values of the anisotropy field. To this end, we define the vector order parameter $\vec{m} = (m_x, m_y) = \frac{1}{L^3}\sum_{\vec{r}}[\cos(\theta_{\vec{r}}), \sin(\theta_{\vec{r}})]$. We measure $\langle |m| \rangle$ (where $|m| \equiv \sqrt{\vec{m}^2}$) and the Binder cumulant $B = \langle (\vec{m}^2)^2 \rangle / \langle \vec{m}^2 \rangle^2$. We also compute the ratio R of correlation functions at fixed distance $R = C_{L/2}/C_{L/4}$, where $C_\ell = \frac{1}{L^3}\sum_{\vec{r}} \langle e^{i\theta_{\vec{r}+\vec{r}_\ell} - i\theta_{\vec{r}}} \rangle$ and $\vec{r}_\ell = (\ell,\ell,\ell)$. The two dimensionless observables B and R are expected to satisfy the standard scaling forms $B = f_B((T - T_c)L^{1/\nu})$ and $R = f_R((T - T_c)L^{1/\nu})$ in the vicinity

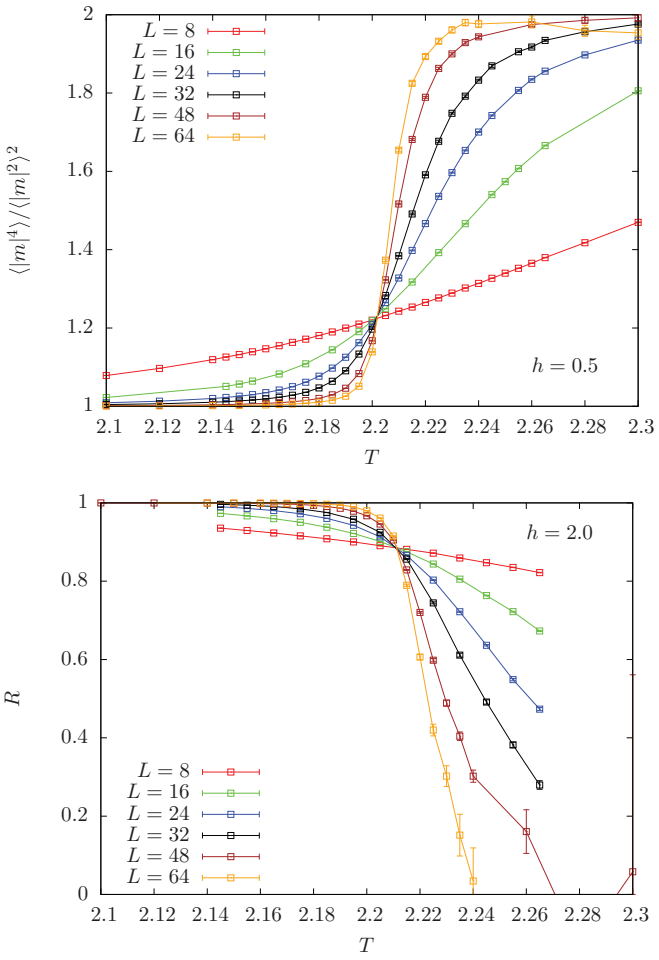

FIG. 7. (Color online) 3d XY model with fourfold anisotropic field: crossing plot for different system sizes for the Binder cumulant B (top panel, for $h = 0.05$) and correlation ratio R (bottom panel crossing plot, for $h = 2$).

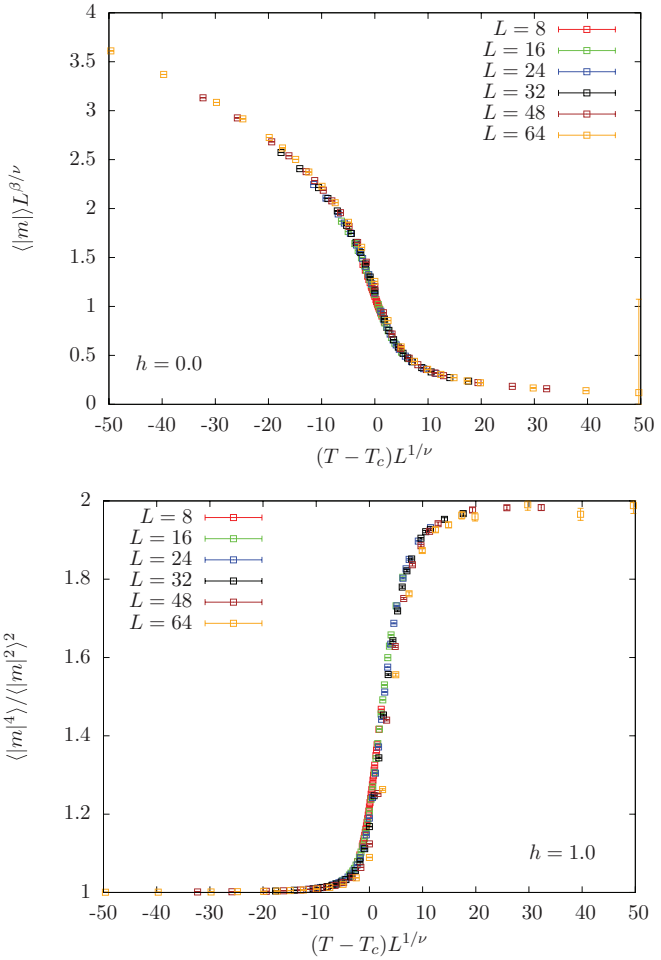

FIG. 8. (Color online) 3d XY model with fourfold anisotropic field: collapse of the order parameter $\langle |m| \rangle$ (top panel, for $h = 0$) and the Binder cumulant B (bottom panel, for $h = 1$), according to the scaling forms mentioned in the text. For estimates on overall error bars, refer to Table II.

of a second-order critical point. Similarly, we also expect the scaling form $\langle |m| \rangle = L^{\beta/\nu} f_m((T - T_c)L^{1/\nu})$.

We employ this strategy at four values of the anisotropy field: $h_4 = 0, 0.5, 1.0, 2.0$, and present typical results for these observables in Figs. 7 and 8. Fitting to the above forms allows us to determine the transition temperature $T_c(h_4)$ reasonably accurately for each of the values of h_4 studied. Results of our fits for $T_c(h_4)$, critical exponents, and amplitudes are given in Table II. They clearly confirm that the universality class of the 3d XY model is unchanged by adding a Z_4 anisotropic field; i.e., it is an irrelevant perturbation at the critical point. Note as well how little T_c changes as a function of h_4.

Armed with this knowledge, we now study W_4, a dimensionless measure of fourfold anisotropy in the vicinity of this critical point. We define it analogously to our definition of W_3 for the Néel-VBS transition: $W_4 = \int d\vec{m}\, P(\vec{m}) \cos(4\theta_m)$ with $P(\vec{m})$ the normalized probability distribution of the order parameter, and $\theta_m = \arctan(m_y/m_x)$ its phase, as measured during the Monte Carlo run. In Fig. 9, we show the size dependence of W_4 close to the critical point for two different values of h_4 (similar results are obtained for the third nonvanishing value of the field studied in our simulations).

Whereas the anisotropy quantifier W_4 increases (towards its limiting value 1) with system size below the critical temperature, it tends to vanish with system size for temperature above T_c. At criticality, the anisotropy W_4 appears to be essentially constant (and nonzero), within our range of system sizes for all nonzero h_4. We also find that this critical value W_{4c} increases significantly with increasing h_4 (see Fig. 9). A finite-size scaling analysis of this behavior, employing some assumptions about the finite-size scaling form, is also reported in Appendix A, and confirms this more elementary analysis. We have also studied (see Appendix B) the analogous quantities for three- and fivefold anisotropies and find that this unusual behavior is specific to the fourfold case.

Our results in the Z_4 case for this better-understood classical problem are thus entirely analogous to our results for W_3 at the Néel-columnar VBS phase boundary. As in that case, this anisotropy coexists with other critical properties being well fitted by standard 3d-XY exponents. Given that Z_4 anisotropy is known to be weakly irrelevant at the three-dimensional XY

TABLE II. Estimates of critical temperature, exponent, and amplitudes resulting from the finite-size scaling analysis of order parameter $\langle|m|\rangle$, Binder cumulants $B = \langle(\vec{m}^2)^2\rangle/\langle\vec{m}^2\rangle^2$, and correlation ratio $R = C_{L/2}/C_{L/4}$. Error bars were determined from the spread on extracted fit parameters depending on critical window size, minimum system sizes included, or degree of polynomial for the universal scaling functions, with χ^2 per degree of freedom always $\lesssim 1.5$.

	$\langle\|m\|\rangle$				Binder ratio B			Correlation ratio R		
h	T_c	ν	β/ν	$f_m(0)$	T_c	ν	$f_B(0)$	T_c	ν	$f_R(0)$
0.0	2.201(1)	0.667(2)	0.515(1)	1.106(6)	2.202(1)	0.675(10)	1.2346(5)	2.202(1)	0.682(9)	0.882(2)
0.5	2.202(1)	0.666(3)	0.51(1)	1.09(5)	2.202(1)	0.676(8)	1.2365(30)	2.203(1)	0.671(1)	0.882(2)
1.0	2.205(1)	0.665(4)	0.514(4)	1.103(10)	2.204(1)	0.671(5)	1.2377(4)	2.205(1)	0.67(1)	0.883(2)
2.0	2.212(1)	0.657(3)	0.520(5)	1.13(2)	2.211(1)	0.6572(10)	1.2458(11)	2.212(1)	0.665(13)	0.884(2)

transition, this leads us to suggest that threefold anisotropy is also weakly irrelevant at the Néel-columnar VBS transition on the honeycomb lattice.

VI. OUTLOOK

We close with a brief discussion of a possible avenue for further progress. It would be desirable to have a model system where the bare value of the threefold anisotropy in the phase of the VBS order parameter ψ could be tuned by hand. This would be analogous to tuning h_4 in the classical three-dimensional XY model.

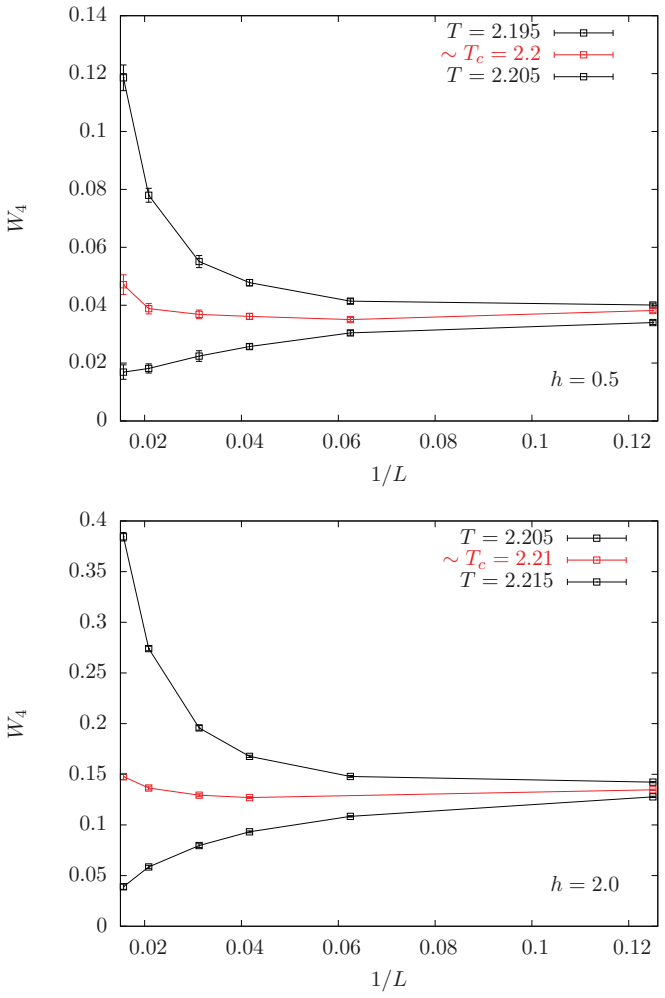

FIG. 9. (Color online) System-size dependence of the anisotropy parameter W_4 close to criticality for three different temperatures: above, below, and very close to the critical temperature T_c. Top panel: $h = 0.5$, bottom panel: $h = 2$.

To achieve this, we begin with the observation that the honeycomb lattice quantum dimer model with ring exchange on hexagonal plaquettes and no interdimer interactions is known [65] to order in a plaquette VBS state, corresponding to the values $(2m+1)\pi/3$ $(m = 0,1,2)$ for the phase of the VBS order parameter ψ. The anisotropy in the phase of ψ in this plaquette-ordered VBS state is thus exactly the opposite of the anisotropy in the columnar-ordered VBS phase (which corresponds to values $2\pi m/3$ for the phase of ψ).

Next, we note that it is possible to write down a six-spin interaction term in an SU(N) spin model which, for large enough N, mimics the ring-exchange term of the honeycomb lattice dimer model. This term, given below, is the honeycomb lattice generalization of similar constructions employed recently [42] on the square lattice:

$$-R_3 \sum_{\langle ijklmn\rangle} [|(ij)(kl)(mn)\rangle\langle(jk)(lm)(ni)| + \text{H.c.}]. \quad (4)$$

Here, the sum is over all such plaquettes of the honeycomb lattice labeled by $\langle ijklmn\rangle$ with vertices labeled cyclically, and $|(ij)(kl)(mn)\rangle$ is the state in which [SU(N)] spins i and j form a [SU(N)] singlet (similarly for spins k and l, and m and n). In the large-N limit, this reduces to a ring-exchange term on each plaquette.

With this motivation, we expect that a nonzero R_3 will counter the columnar phase anisotropy seen at the critical point of the SU(2)-invariant J-Q_3 model and allow us to tune the value of W_3 while leaving other critical properties unchanged. Thus, we conjecture that the SU(2)-invariant J-Q_3-R_3 model (employing the R_3 term defined above) provides a promising setting in which one can tune the bare value of the anisotropy in the phase of ψ, and explicitly check the idea that this threefold anisotropy is a weakly irrelevant variable at the Néel-columnar VBS transition. In addition, it may even be possible to change the character of the ordered state (from columnar to plaquette VBS) if R_3 dominates over Q_3. It should be possible to confirm these ideas using projector QMC simulations of this J-Q_3-R_3 model, and we hope to return to this in future work.

ACKNOWLEDGMENTS

This work was made possible by research support from the Indo-French Centre for the Promotion of Advanced Research (IFCPAR/CEFIPRA) under Project No. 4504-1 and DST Grant No. DST-SR/S2/RJN-25/2006, and performed using computational resources from GENCI (Grant No. x2014050225), CALMIP (Grant No. 2014-P0677), and the Department of Theoretical Physics of the TIFR. S.P. is grateful to the Department of Theoretical Physics of the TIFR for hospitality during part of this work. In the final stages of this work, S.P. was also supported by CAREER award NSF DMR-1056536.

APPENDIX A: FINITE-SIZE SCALING ANALYSIS OF THE DIMENSIONLESS ANISOTROPY QUANTIFIER

To supplement the W_3 versus L behavior at fixed Q_2 that we looked at in the main text, we perform a finite-size scaling analysis based on the scaling theory of Lou *et al.* [26]. Reference [26] studied the classical 3d XY model in the presence of a Z_q anisotropy field, which is a dangerously irrelevant operator at criticality for $q \geqslant 4$, and proposed a scaling form for the dimensionful anisotropy order parameter as $\langle m_q \rangle = L^{-\beta/\nu} f_{m_q}((T - T_c)L^{1/\nu_q})$, an extension of the XY order parameter scaling form $\langle m \rangle = L^{-\beta/\nu} f_m((T - T_c)L^{1/\nu})$. ν_q is the exponent associated with a length scale below which the order parameter distribution appears isotropic, even below

TABLE III. Results of finite-size scaling analysis for the dimensionless anisotropy quantifier W_3 for the J-Q_2-Q_3 model. Error bars were determined again using the same protocol as in Sec. IV A of the main text (see Table I).

Q_2	Q_{3c}	ν_3	$g_{W_3}(0)$
0.0	1.183(2)	0.57(2)	0.115(6)
0.14	1.485(1)	0.58(1)	0.120(3)
0.60	2.485(1)	0.56(2)	0.129(2)
0.85	3.027(2)	0.56(2)	0.128(3)
20.0	45.00(3)	0.57(1)	0.134(2)

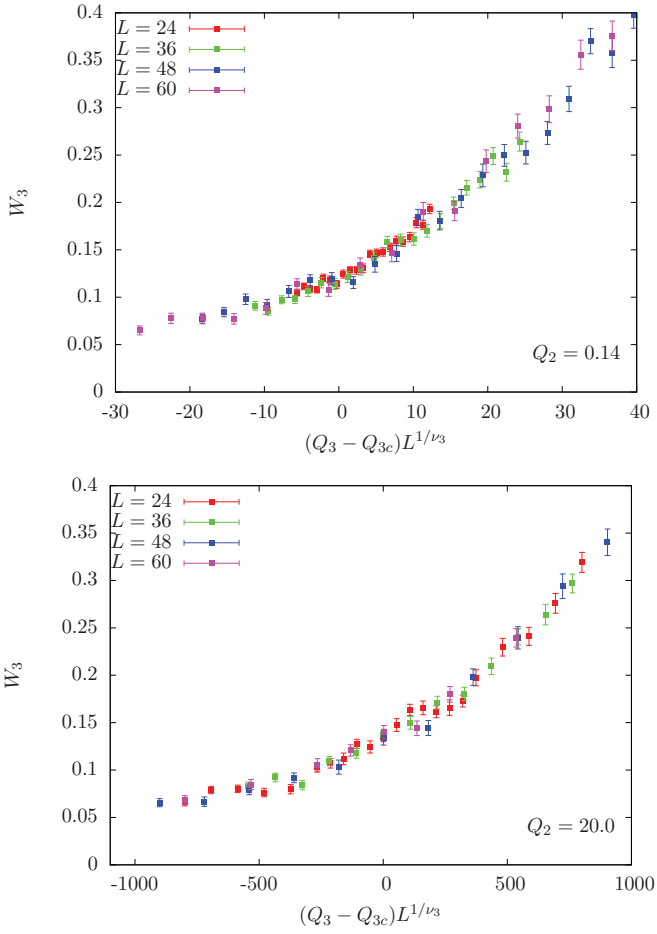

FIG. 10. (Color online) Scaling collapse plots according to the scaling form $W_3 = g_{W_3}((Q_3 - Q_{3c})L^{1/\nu_3})$ for the dimensionless anisotropy quantifier W_3 in the J-Q_2-Q_3 model for $Q_2 = 0.14$ (top panel) and $Q_2 = 20$ (bottom panel). For the fits, similar to Sec. IV A, a particular choice of critical window, minimum system size included, and order of universal function was taken here which gave χ^2 per degree of freedom equal to 1.26 and 1.31 for the plots respectively.

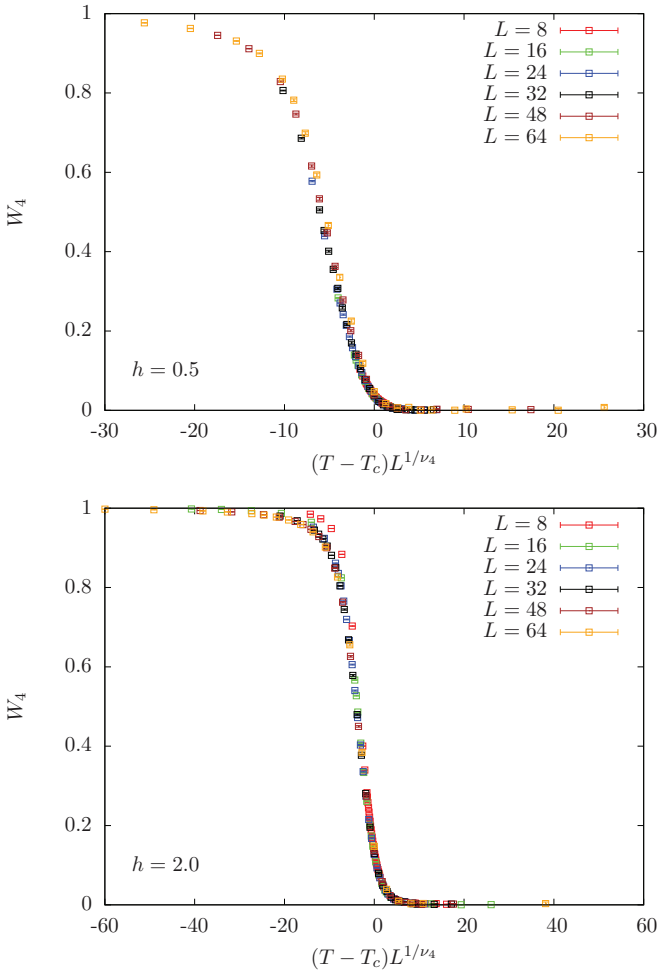

FIG. 11. (Color online) Scaling collapse plots according to the scaling form $W_4 = g_{W_4}((T - T_c)L^{1/\nu_4})$ for the dimensionless anisotropy quantifier W_4 in the 3d XY model with fourfold anisotropy field for $h = 0.5$ (top panel) and $h = 2$ (bottom panel). For estimates on overall error bars, refer to Table IV.

TABLE IV. Results of finite-size scaling analysis for anisotropy quantifier W_4 for the 3d XY model with fourfold anisotropic field. Error bars were determined with the same procedure as in the main text (see Table I).

h	T_c	ν_4	$f_{W_4}(0)$
0.5	2.202(2)	0.76(10)	0.031(4)
1.0	2.204(1)	0.70(2)	0.062(4)
2.0	2.211(1)	0.665(20)	0.120(1)

T_c. We have $\nu_q > \nu$, as this length scale diverges faster than the ferromagnetic correlation length (see the analogy with the VBS anisotropy length scale in the theory of deconfined criticality [14,15]). Reference [26] related ν_q/ν to the scaling dimension of the anisotropy field, but we note that in a recent work this relation was questioned [64].

J-Q_2-Q_3 model. In our case of the dimensionless anisotropy order parameter W_3, we can assume following Ref. [26] a similar scaling form $g_{W_3}((Q_3 - Q_{3c})L^{1/\nu_3})$ for fixed Q_2, without further assumption on ν_3. Figure 10 shows examples of this scaling analysis and Table III summarizes the results of the corresponding fits.

We see that the critical point Q_{3c} extracted from the scaling analysis is again in agreement with those gotten from other analyses (Sec. IV A). We again find the same conclusions as that from visual inspection of W_3 versus L behavior: there is a finite value of $W_{3c} = g_{W_3}(0)$ at the critical point for all Q_2, which furthermore seems to slightly increase with Q_2. Finally, within our precision, it is not possible to positively confirm that the extracted value of ν_3 is larger than ν (the two exponents are essentially equal within error bars): independent of the exact relation between the two [26,64], this indicates that threefold anisotropy is only very slightly irrelevant, consistent with a nonvanishing W_{3c} within our system size range.

3d XY model with fourfold anisotropy field. We perform the same analysis for the anisotropy quantifier W_4 of the 3d XY model. In Fig. 11, we show the scaling collapse for W_4 with the scaling form $W_4 = g_{W_4}((T - T_c)L^{1/\nu_4})$ as the anisotropy field h_4 is varied. Table IV summarizes the results of the scaling analyses.

We find again the critical temperature T_c is in agreement with those extracted from other order parameters (Sec. V) and changes very little with h_4, as already mentioned. This analysis confirms that W_4 takes a clearly nonzero value $W_{4c} = f_{W_4}(0)$ at the critical point, which logically increases with h_4. In this case, we are able to confirm that $\nu_4 > \nu$ as found in Ref. [26] except for the largest field $h = 2$ where this relation is only marginally verified (this can be expected as we probably need larger systems when anisotropy is stronger).

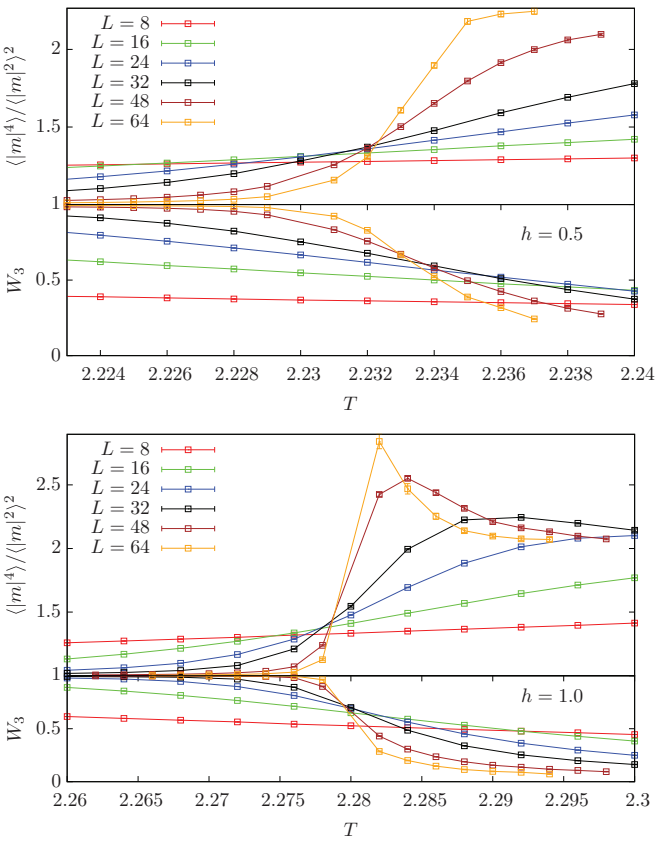

FIG. 12. (Color online) 3d XY model with threefold anisotropic field: temperature dependence of the Binder cumulant (top panels) and threefold anisotropy quantifier W_3 (bottom panels) for two different values of $h_3 = 0.5, 1.0$.

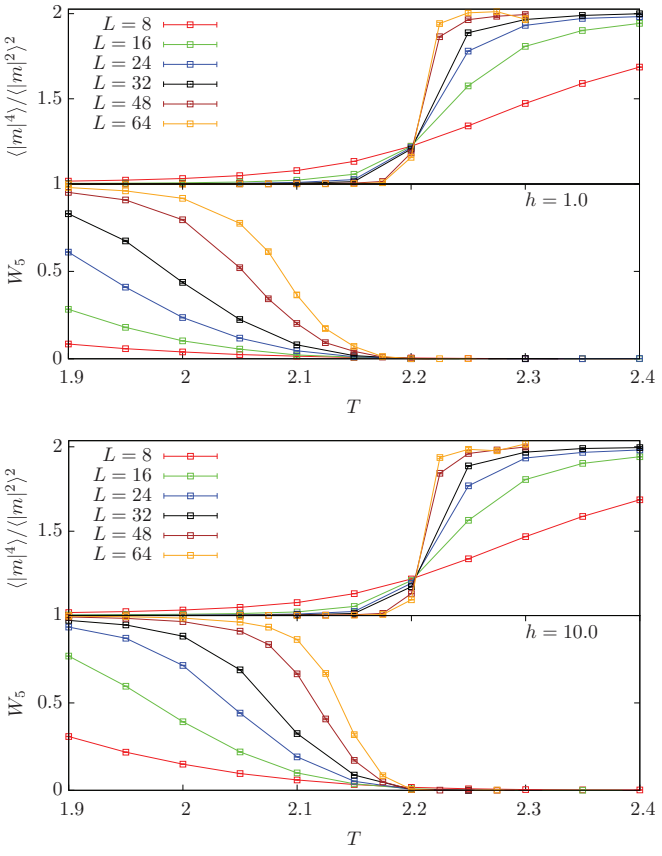

FIG. 13. (Color online) 3d XY model with fivefold anisotropic field: temperature dependence of the Binder cumulant (top panels) and fivefold anisotropy quantifier W_5 (bottom panels) for two different values of $h_5 = 1, 10$.

APPENDIX B: 3d *XY* MODEL WITH THREE- AND FIVEFOLD ANISOTROPIC FIELDS

Here we show that a nearly constant critical anisotropy is specific to the 3d *XY* model with fourfold anisotropic field by studying the same model with a three- and fivefold anisotropy field, replacing the term $-h_4 \sum_{\vec{r}} \cos(4\theta_{\vec{r}})$ by $-h_q \sum_{\vec{r}} \cos(q\theta_{\vec{r}})$ with $q = 3,5$ in Eq. (3). We again compute the Binder cumulant and the anisotropy quantifiers W_3 and W_5 adapting the above definitions.

$q = 3$ *case*. We know that the anisotropy is relevant here, rendering the transition first order. This is clearly seen in the top panels of Fig. 12 where, for two different field values, the Binder cumulant show significant drifts in the crossing point between two consecutive sizes. The bottom panels show the temperature dependence of W_3, which also show drifting pseudocrossing points. The clear increase with L of W_3 nearest to the transition temperature where the pseudocrossing in the Binder cumulant is located indicates that anisotropy is relevant at criticality. Note as well how the value of T_c is substantially modified by h_3.

$q = 5$ *case*. Anisotropy is irrelevant here and the second-order nature of the transition is revealed by the nice monotonic crossing behavior of the Binder cumulant in the top panels of Fig. 13 for two different values of h_5. There is no observable drift in T_c even when h_5 changes by a factor of 10; in fact, one observes that the Binder cumulant are essentially the same, indicating the strong irrelevancy of fivefold anisotropy. The bottom panels of Fig. 13 show the size and temperature dependence of W_5, which as expected clearly goes to zero at the critical point. We performed a finite-size scaling analysis of the data (not shown) which yield the expected results, such as nondrifting T_c, $\nu_5 > \nu$, $f_{W_5}(0) = 0$, and the correct 3d *XY* value for ν.

[1] A. Auerbach, *Interacting Electrons and Quantum Magnetism* (Springer Verlag, New York, 1994).
[2] Martin P. Gelfand, Rajiv R. P. Singh, and David A. Huse, Phys. Rev. B **40**, 10801 (1989).
[3] M. Mambrini, A. Läuchli, D. Poilblanc, and F. Mila, Phys. Rev. B **74**, 144422 (2006).
[4] A. F. Albuquerque, D. Schwandt, B. Hetényi, S. Capponi, M. Mambrini, and A. M. Läuchli, Phys. Rev. B **84**, 024406 (2011).
[5] Z. Zhu, D. A. Huse, and S. R. White, Phys. Rev. Lett. **110**, 127205 (2013).
[6] R. Ganesh, J. van den Brink, and S. Nishimoto, Phys. Rev. Lett. **110**, 127203 (2013).
[7] S.-S. Gong, D. N. Sheng, O. I. Motrunich, and M. P. A. Fisher, Phys. Rev. B **88**, 165138 (2013).
[8] S.-S. Gong, W. Zhu, D. N. Sheng, O. I. Motrunich, and M. P. A. Fisher, Phys. Rev. Lett. **113**, 027201 (2014).
[9] R. K. Kaul, R. G. Melko, and A. W. Sandvik, Annu. Rev. Condens. Matter Phys. **4**, 179 (2013).
[10] S. Sachdev and M. Vojta, J. Phys. Soc. Jpn. **69**, Suppl. B, 1 (2000).
[11] L. D. Landau, E. M. Lifshitz, and E. M. Pitaevskii, *Statistical Physics* (Butterworth-Heinemann, New York, 1999).
[12] A. Sen and A. W. Sandvik, Phys. Rev. B **82**, 174428 (2010).
[13] A. Banerjee, K. Damle, and A. Paramekanti, Phys. Rev. B **83**, 134419 (2011).
[14] T. Senthil, L. Balents, S. Sachdev, A. Vishwanath, and M. P. A. Fisher, Phys. Rev. B **70**, 144407 (2004).
[15] T. Senthil, A. Vishwanath, L. Balents, S. Sachdev, and M. P. A. Fisher, Science **303**, 1490 (2004).
[16] M. Levin and T. Senthil, Phys. Rev. B **70**, 220403 (2004).
[17] F. D. M. Haldane, Phys. Rev. Lett. **61**, 1029 (1988).
[18] N. Read and S. Sachdev, Phys. Rev. Lett. **62**, 1694 (1989).
[19] N. Read and S. Sachdev, Phys. Rev. B **42**, 4568 (1990).
[20] A. D'Adda, P. Di Vecchia, and M. Luscher, Nucl. Phys. B **146**, 63 (1978); E. Witten, *ibid.* **149**, 285 (1979); S. Coleman, Ann. Phys. (N.Y.) **101**, 239 (1976).
[21] O. I. Motrunich and A. Vishwanath, Phys. Rev. B **70**, 075104 (2004).
[22] M.-h. Lau and C. Dasgupta, J. Phys. A **21**, L51 (1988); Phys. Rev. B **39**, 7212 (1989).
[23] M. Kamal and G. Murthy, Phys. Rev. Lett. **71**, 1911 (1993).
[24] S. Sachdev and R. A. Jalabert, Mod. Phys. Lett. B **4**, 1043 (1990).
[25] M. Oshikawa, Phys. Rev. B **61**, 3430 (2000).
[26] J. Lou, A. W. Sandvik, and L. Balents, Phys. Rev. Lett. **99**, 207203 (2007).
[27] W. Janke and R. Villanova, Nucl. Phys. B **489**, 679 (1997).
[28] M. S. Block, R. G. Melko, and R. K. Kaul, Phys. Rev. Lett. **111**, 137202 (2013).
[29] A. W. Sandvik, Phys. Rev. Lett. **98**, 227202 (2007).
[30] R. G. Melko and R. K. Kaul, Phys. Rev. Lett. **100**, 017203 (2008).
[31] F. J. Jiang, M. Nyfeler, S. Chandrasekharan, and U. J. Wiese, J. Stat. Mech.: Theory Exp. (2008) P02009.
[32] K. S. D. Beach, F. Alet, M. Mambrini, and S. Capponi, Phys. Rev. B **80**, 184401 (2009).
[33] J. Lou, A. W. Sandvik, and N. Kawashima, Phys. Rev. B **80**, 180414 (2009).
[34] A. W. Sandvik, Phys. Rev. Lett. **104**, 177201 (2010).
[35] A. Banerjee, K. Damle, and F. Alet, Phys. Rev. B **82**, 155139 (2010).
[36] R. K. Kaul, Phys. Rev. B **84**, 054407 (2011).
[37] A. Banerjee, K. Damle, and F. Alet, Phys. Rev. B **83**, 235111 (2011).
[38] R. K. Kaul, Phys. Rev. B **85**, 180411(R) (2012).
[39] R. K. Kaul and A. W. Sandvik, Phys. Rev. Lett. **108**, 137201 (2012).
[40] A. W. Sandvik, Phys. Rev. B **85**, 134407 (2012).
[41] S. Jin and A. W. Sandvik, Phys. Rev. B **87**, 180404 (2013).
[42] R. K. Kaul, Phys. Rev. B **91**, 054413 (2015).
[43] S. Pujari, K. Damle, and F. Alet, Phys. Rev. Lett. **111**, 087203 (2013).
[44] K. Harada, T. Suzuki, T. Okubo, H. Matsuo, J. Lou, H. Watanabe, S. Todo, and N. Kawashima, Phys. Rev. B **88**, 220408(R) (2013).
[45] K. Chen, Yuan Huang, Youjin Deng, A. B. Kuklov, N. V. Prokof'ev, and B. V. Svistunov, Phys. Rev. Lett. **110**, 185701 (2013).
[46] O. I. Motrunich and A. Vishwanath, arXiv:0805.1494.

[47] A. B. Kuklov, M. Matsumoto, N. V. Prokof'ev, B. V. Svistunov, and M. Troyer, Phys. Rev. Lett. **101**, 050405 (2008).
[48] G. J. Sreejith and S. Powell, Phys. Rev. B **89**, 014404 (2014).
[49] D. Charrier and F. Alet, Phys. Rev. B **82**, 014429 (2010).
[50] S. Powell and J. T. Chalker, Phys. Rev. B **80**, 134413 (2009).
[51] G. Chen, J. Gukelberger, S. Trebst, F. Alet, and L. Balents, Phys. Rev. B **80**, 045112 (2009).
[52] S. Powell and J. T. Chalker, Phys. Rev. Lett. **101**, 155702 (2008).
[53] D. Charrier, F. Alet, and P. Pujol, Phys. Rev. Lett. **101**, 167205 (2008).
[54] G. Misguich, V. Pasquier, and F. Alet, Phys. Rev. B **78**, 100402(R) (2008).
[55] F. Alet, G. Misguich, V. Pasquier, R. Moessner, and J. L. Jacobsen, Phys. Rev. Lett. **97**, 030403 (2006).
[56] R. K. Kaul and R. G. Melko, Phys. Rev. B **78**, 014417 (2008).
[57] F. S. Nogueira and A. Sudbo, Phys. Rev. B **86**, 045121 (2012).
[58] L. Bartosch, Phys. Rev. B **88**, 195140 (2013).
[59] J. Lee and S. Sachdev, Phys. Rev. B **90**, 195427 (2014).
[60] M. Hasenbusch and E. Vicari, Phys. Rev. B **84**, 125136 (2011).
[61] A. W. Sandvik and H. G. Evertz, Phys. Rev. B **82**, 024407 (2010).
[62] K. Vollmayr, J. D. Reger, M. Scheucher, and K. Binder, Z. Phys. B **91**, 113 (1993).
[63] U. Wolff, Phys. Rev. Lett. **62**, 361 (1989).
[64] T. Okubo, K. Oshikawa, H. Watanabe, and N. Kawashima, arXiv:1411.1872.
[65] R. Moessner, S. L. Sondhi, and P. Chandra, Phys. Rev. B **64**, 144416 (2001).
[66] Reference [42] recently found a similar critical Néel-VBS line on the square lattice, but did not test for universality.